PNAS RESEARCH ARTICLE | PHYSIOLOGY | BIOPHYSICS AND COMPUTATIONAL BIOLOGY
OPEN ACCESS

Distributed propulsion enables fast and efficient swimming modes in physonect siphonophores

Kevin T. Du Clos[a,1,2], Brad J. Gemmell[a], Sean P. Colin[b,c], John H. Costello[c,d], John O. Dabiri[e], and Kelly R. Sutherland[f]

Edited by M. Koehl, University of California, Berkeley, CA; received February 10, 2022; accepted October 25, 2022

Many fishes employ distinct swimming modes for routine swimming and predator escape. These steady and escape swimming modes are characterized by dramatically differing body kinematics that lead to context-adaptive differences in swimming performance. Physonect siphonophores, such as *Nanomia bijuga*, are colonial cnidarians that produce multiple jets for propulsion using swimming subunits called nectophores. Physonect siphonophores employ distinct routine and steady escape behaviors but—in contrast to fishes—do so using a decentralized propulsion system that allows them to alter the timing of thrust production, producing thrust either synchronously (simultaneously) for escape swimming or asynchronously (in sequence) for routine swimming. The swimming performance of these two swimming modes has not been investigated in siphonophores. In this study, we compare the performances of asynchronous and synchronous swimming in *N. bijuga* over a range of colony lengths (i.e., numbers of nectophores) by combining experimentally derived swimming parameters with a mechanistic swimming model. We show that synchronous swimming produces higher mean swimming speeds and greater accelerations at the expense of higher costs of transport. High speeds and accelerations during synchronous swimming aid in escaping predators, whereas low energy consumption during asynchronous swimming may benefit *N. bijuga* during vertical migrations over hundreds of meters depth. Our results also suggest that when designing underwater vehicles with multiple propulsors, varying the timing of thrust production could provide distinct modes directed toward speed, efficiency, or acceleration.

locomotion | biomechanics | efficiency

Significance

Siphonophores are colonial cnidarians that, unlike single jetters such as squids, swim using propulsion from multiple jets, produced using subunits called nectophores. Distributing propulsion spatially provides advantages in redundancy and maneuverability, and distributing propulsion over time enables context-adaptive swimming modes. We use experiments and modeling to compare swimming modes. We show that synchronous swimming produces high mean speeds and accelerations. By contrast, asynchronous swimming consumes less energy. Thus, by simple variations to the timing of thrust production, siphonophores achieve similar functionality to that of fishes, the ability to adapt swimming performance to context. A greater understanding of the benefits of multijet propulsion may also improve underwater vehicle design.

Pulsed jets are an efficient, convergent solution to swimming propulsion for a broad taxonomic range of marine organisms, including cnidarians, cephalopods, and pelagic tunicates (1, 2). Swimming through the use of multiple pulsed jets is much less common. The "multijet" swimming strategy is found in only two taxa of marine swimmers, siphonophores and the taxonomically distant salps (3), but distributed propulsion has the advantage of allowing thrust to be distributed spatially and temporally. Varying the spatial distribution of thrust enhances maneuverability—a swimmer can turn quickly by focusing thrust near the end of a lever arm (4), provides redundancy in case of failure by one or more propulsive units, and facilitates the production of power in excess of what a single propulsor could produce (5). Varying the temporal distribution of thrust by pulsing jets independently could provide additional swimming performance benefits, but these effects have not been well studied. In this study, we examine the effects of thrust timing and the number of propulsors on swimming performance.

Nanomia bijuga is a widely distributed physonect siphonophore (6). Inhabiting depths from the sea surface to at least 800 m, *N. bijuga* performs twice daily migrations of hundreds of meters (6, 7) and is an important predator on crustaceans in some regions (8); in Monterey Bay, it is the dominant gelatinous organism at midwater depths (9, 10). Siphonophores are an order of colonial marine cnidarians; physonect siphonophores have the most complex modular architecture of any colonial organism with highly specialized individuals called zooids (11–13). The siphosome is composed of repeating arrays of zooids specialized for prey capture and digestion, defense, reproduction, and other functions (Fig. 1*A* and Figure 6A in ref. 6). The carbon monoxide-filled pneumatophore (14, 15) at the apex of the colony regulates buoyancy and controls vertical orientation. Propulsion is produced by the nectosome, which comprises two rows of specialized swimming zooids called nectophores. Each nectophore produces a jet by alternate expansions and contractions that direct currents through a thin, flexible aperture called the velum (16, Fig. 1*B*).

Four nectophore contraction patterns have been identified for *N. bijuga*: 1) synchronous contraction of all of the nectophores in a colony, 2) asynchronous contractions

Author contributions: K.T.D. and K.R.S. designed research; K.T.D., B.J.G., S.P.C., J.H.C., and K.R.S. performed research; K.T.D. and J.O.D. contributed new reagents/analytic tools; K.T.D. analyzed data; and K.T.D. wrote the paper.

The authors declare no competing interest.

This article is a PNAS Direct Submission.

[1]To whom correspondence may be addressed. Email: kduclos@lumcon.edu.

[2]Present address: Louisiana Universities Marine Consortium, Chauvin, LA 70344.

This article contains supporting information online at http://www.pnas.org/lookup/suppl/doi:10.1073/pnas.2202494119/-/DCSupplemental.

Published November 29, 2022.

... metabolic plasticity of breast cancer

Ren, Zuen Liang, Huizhi Galbo, Phillip M. Jr. Dharmaratne, Malindrie Kulkarni, Ameya S. Fard, Atefeh Taherian Louise Aoun, Marie Martinez-Lopez, Nuria Suyama, Kimita Benard, Outhiriaradjou Zheng, Wei Liu, Yang Albanese, Joseph Zheng, Deyou Mar, Jessica C. Singh, Rajat Prystowsky, Michael B. Norton, Larry Hazan and Rachel B. [a,b,c,d,e,f,g,h,i,1]

breast cancer | progression | glutathione peroxidase 2 | reactive oxygen species | hypoxia | HIF1α | VEGFA | angiogenesis | oxidative phosphorylation | glycolysis | scRNA-seq | metabolic plasticity

Tumor cell hyperproliferation results in cell crowding causing nutrients and oxygen deprivation, leading to hypoxia (1). To meet the energetic demands of cancer cells, mitochondria consume the cellular oxygen, resulting in oxidative phosphorylation, leading to reactive oxygen species (ROS) production (2).

While low to mild ROS levels promote oncogenic signaling and malignancy, high levels of ROS cause DNA damage and apoptosis (3, 4), an effect that is often co-opted by chemotherapy or radiation to target cancer cells (5). Tumor cells evade ROS cytotoxicity by increasing the expression of antioxidant enzymes such as superoxide dismutase, peroxiredoxin-thioredoxin, catalases, and glutathione peroxidases (6, 7), which generally convert hydrogen peroxide produced by mitochondrial electron leak into water using glutathione (8).

ROS are known to stimulate oncogenic signaling with special emphasis on hypoxia-inducible factor 1-alpha (HIF1α). ROS stabilize HIF1α protein via inhibition of the oxygen-sensing propyl hydroxylase protein D (PHD), which normally marks HIF1α for proteasomal degradation (9, 10). HIF1α promotes malignancy via effects on tumor angiogenesis, proliferation, epithelial-to-mesenchymal transition, stemness, and glucose metabolism (1, 11). HIF1α stimulates VEGFA gene transcription which promotes angiogenesis, thereby increasing nutrient availability and oxygen supply to hypoxic tumor areas (12, 13). Paradoxically, VEGFA overproduction may also cause vascular malfunction, resulting in immature or poorly perfusing vessels, thereby exacerbating hypoxia (14). This further stabilizes HIF1α protein, which shifts cells from oxidative phosphorylation (OXPHOS) to aerobic glycolysis, known as the Warburg effect (12, 15). While OXPHOS generates high levels of ATP as compared to glycolysis, tumor cells leverage glucose metabolism to generate building blocks for biomass biosynthesis (16). However, aggressive cancer cells were also shown to be able to use OXPHOS and glycolysis, which might be necessary to survive under hypoxic and aerobic conditions that can be encountered at the primary tumor, in circulation, or at metastatic sites (17, 18).

A comparison of carcinoma cell lines derived from the polyoma middle T (PyMT) mammary tumor model unraveled a dramatic downregulation of glutathione peroxidase 2 (GPx2) in metastatic relative to non-metastatic cells from the parental tumor. Moreover, the loss of GPx2 in several molecular breast cancer (BC) subtypes was correlated with poor patient survival, underscoring the clinical significance of GPx2 loss in BC. GPx2 knockdown (KD) in murine and human BC cells stimulates ROS/HIF1α/VEGFA signaling which enhanced malignant progression via vascular modulation, resulting in poor perfusion, hypoxia, and a shift from OXPHOS to aerobic glycolysis (the Warburg effect). Transcriptomic analysis of scRNA-seq data and bioenergetic profiling confirmed that

The authors declare no competing interest.

This article contains supporting information online at XXX.

To whom correspondence may be addressed. Email: gail.mccain883@gmail.com

Received 31 March 2022; Accepted 31 March 2022

PNAS 2022 Vol. XX No. XX e2202494119 https://doi.org/10.1073/pnas.2202494119 1 of 15

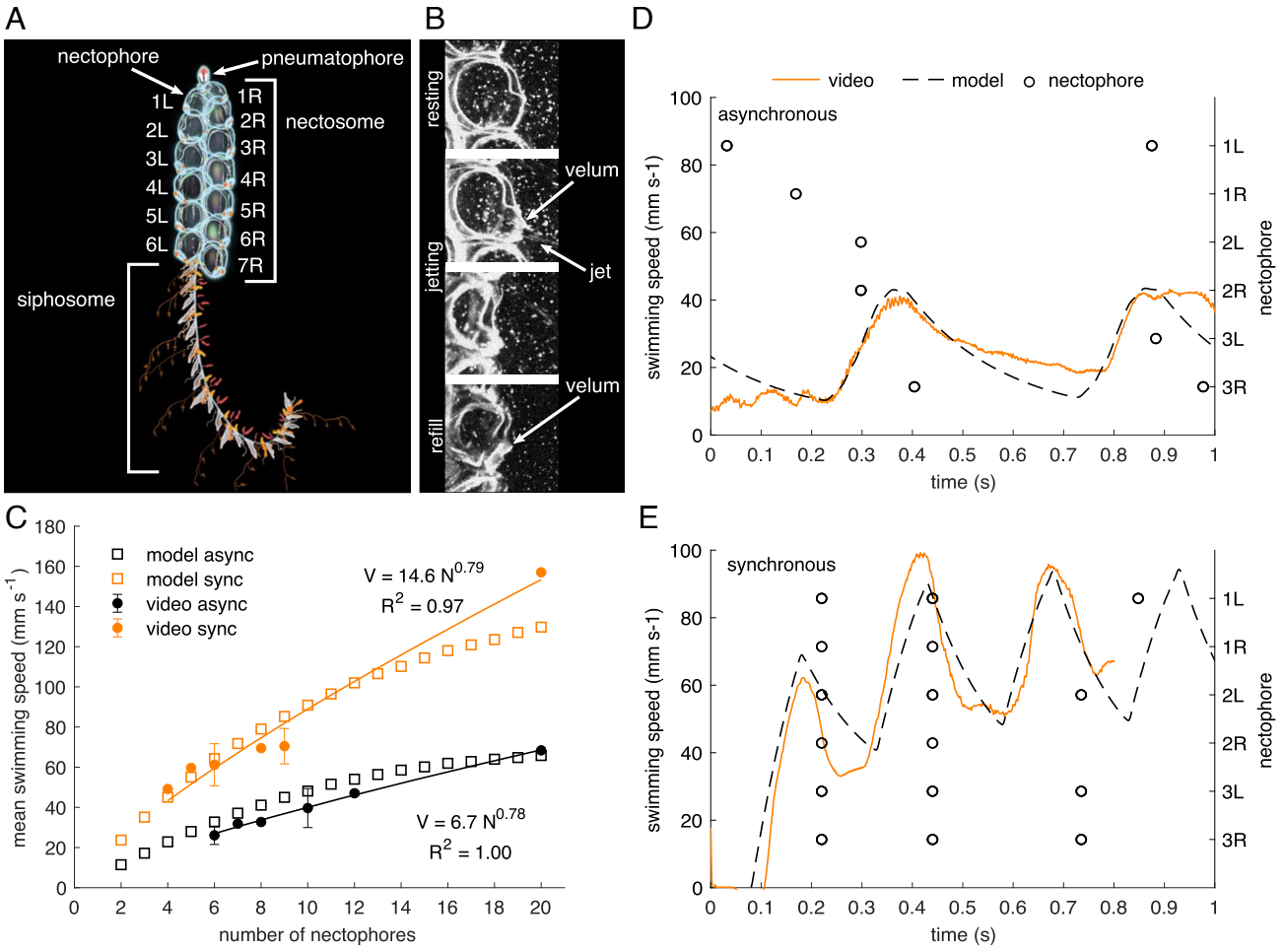

Fig. 1. Measured and modeled swimming speeds. (*A*) Illustration of *N. bijuga*, indicating relevant morphological features. (*B*) Detail of one nectophore, showing the sequence of jetting and refill and the locations of the velum and jet. (*C*) Comparison of modeled and measured mean swimming speeds vs. colony length. For measured swimming speeds, means and standard deviations by nectophore count of swimming speed from videos are shown along with power law fits (n = 13 asynchronous and 11 synchronous colonies). (*D* and *E*) Instantaneous swimming speeds for asynchronous and synchronous swimming. Circles indicate times of the maximum nectophore contraction with the side of the colony (left or right on the video) and the nectophore number (starting at the apical end) indicated.

in which nectophores are fired sequentially—generally starting at the apex and progressing down in pairs, 3) synchronous contraction of the nectophores on one side of the colony, and 4) contraction of an individual nectophore (13). Contraction patterns (3) and (4) are used in turning and enable *N. bijuga* to rotate with a high angular velocity and tight turning radius (4). This study focuses on the first two contraction patterns, which are used in forward swimming (synchronous propulsion is also used in reverse swimming).

Many fishes employ distinct kinematics depending on whether they are swimming steadily or attempting to escape a predator (17), with steady swimming favoring efficiency and escape swimming favoring acceleration at the expense of efficiency (18). Analogously, *N. bijuga* likely uses asynchronous propulsion during routine steady swimming and vertical migrations over hundreds of meters depth (7, 19) and uses synchronous swimming during escape swimming, which could aid in evading predators, such as narcomedusae (20). It is unknown, however, whether each mode has swimming performance characteristics adaptive to the distinct requirements of the associated behavior, as is the case for fishes.

Using experimental data and a mechanistic swimming model, we compare swimming performances of asynchronous and synchronous modes for *N. bijuga* colonies of varying lengths, i.e., numbers of nectophores. We show that synchronous propulsion produces higher swimming speeds and accelerations than asynchronous propulsion but with a higher cost of transport. *N. bijuga* uses its multiple propulsors to switch between swimming modes adaptive for long-distance and routine swimming (asynchronous) or escape swimming (synchronous).

Results

To determine the effects of swimming mode and colony length on *N. bijuga* swimming performance, we developed a mechanistic one-dimensional swimming model that incorporates swimming parameters derived from experimental data. The model solves the unsteady equation of motion in the vertical (swimming) direction with a time-varying thrust component for each nectophore in a colony (see *Methods* section for details). Model parameters were measured from videos of *N. bijuga* swimming in the laboratory or derived from the literature (Table 1).

Starting with measured and estimated parameters (Table 1), we varied thrust and drag parameters in the model in asynchronous and synchronous swimming modes to approximate measured mean, minimum, and maximum swimming speeds across colony

Table 1. Estimated swimming parameters

Parameter	Symbol	Value	Units
Number of nectophores	N	2–20	
Nectosome length	L	$1.64 \cdot N + 0.68$	mm
Nectosome diameter	D	5.5	mm
Max. swimming speed	V_{max}	$16.33 \cdot N + 11.71$	mm s^{-1}
Jetting thrust per nectophore	F_{tj}	60	μN
Refill thrust per nectophore	F_{tr}	6	μN
Maximum jet speed	v_{max}	908	mm s^{-1}
Max. jet speed vs. thrust	v_{max}	$68.52 \cdot F_{tj}^{0.5}$	mm s^{-1}
Animal density	ρ	1,022	kg m^{-3}
Pulse frequency	f	3	Hz
Jetting time	T_j	0.1	s
Refill time	T_r	0.1	s
Drag coefficient	C_d	Eq. **3**	
Added mass coefficient	α	0.1	
Fluid density	ρ_f	1,020	kg m^{-3}
Fluid dynamic viscosity	μ	1×10^{-3}	Pa s

Base parameters used to initialize the model.

lengths (*SI Appendix*, Table S1 and Fig. 1*C*). For subsequent model runs, we tested three cases: asynchronous and synchronous modes with their respective parameters and asynchronous-matched, in which the model was run in asynchronous mode but with thrust and drag parameters matched to the synchronous mode. The latter case was used to isolate the effects of individual nectophore kinematics and pulse timing (asynchronous vs. synchronous).

To verify that the model approximates realistic swimming behavior in both asynchronous and synchronous modes, we also tuned the model for individual video sequences by varying thrust, drag, mass, and pulse frequency. In both the videos and the model, asynchronous swimming produced smoother, more gradual accelerations than synchronous swimming (Figs. 1 *D* and *E* and 2).

Swimming Kinematics. Based on video data, synchronous swimming was faster than asynchronous swimming for all colony lengths, with the greatest differences for the longest colonies (Fig. 1*B*). For a colony with 20 nectophores, the mean swimming speed for synchronous swimming was more than double that for asynchronous swimming (157.0 vs. 65.4 mm s^{-1}). For synchronous swimming, mean swimming speed increased threefold over the range of colony lengths measured, from 49 mm s^{-1} for a colony with 4 nectophores to 157 mm s^{-1} for a colony with 20 nectophores. The relationships between swimming speed and nectophore count were well described by power law fits for both synchronous ($V = 14.6N^{0.79}$; $R^2 = 0.97$; $n = 9$) and asynchronous ($V = 6.7N^{0.78}$; $R^2 = 1.00$ $n = 13$) swimming. Mean swimming speeds were also significantly slower for the same colony swimming asynchronously vs. synchronously (*t*-test $p = 0.02$; $n = 3$).

Modeled and measured mean swimming speeds were similar (Figs. 1*C* and 3*A*), but for synchronous swimming, the model slightly underestimated swimming speeds for the longest colonies. Acceleration increased with colony length for synchronous swimming but gradually decreased for asynchronous swimming. Synchronous swimming in the model yielded initial accelerations 2.0–6.3 times as great as for asynchronous swimming (Fig. 3*B*). From the model, swimming Reynolds numbers based on nectosome length and maximum speed ranged from ∼100 to 2,590 for asynchronous and ∼210–5,810 for synchronous swimming (*SI Appendix*, Fig. S1*A*).

When parameters were matched in the model (asynchronous-matched case), mean swimming speeds for asynchronous and synchronous swimming were nearly identical, demonstrating that the observed difference in swimming speeds was due almost entirely to differences in total thrust and drag rather than differences in the timing of thrust production (Fig. 3*A*). In contrast, the timing of thrust production was important for acceleration; the relationship between colony length and acceleration for the asynchronous-matched case was more similar to the asynchronous than to the synchronous case (Fig. 3*B*).

Thrust and Drag. We investigated the causes of the observed differences in swimming speeds between asynchronous and

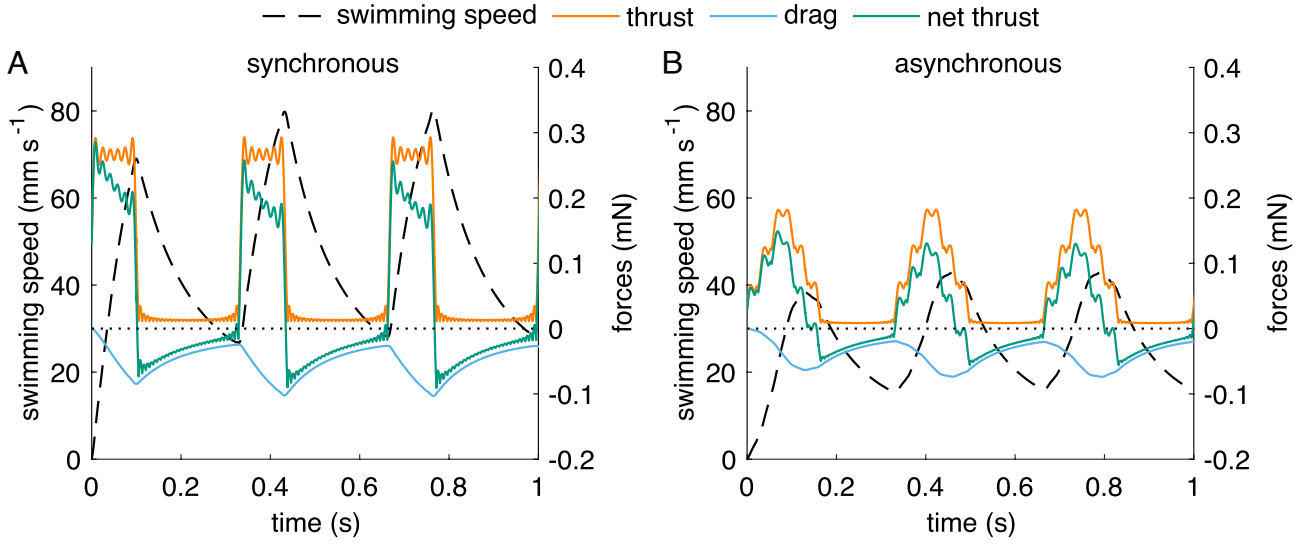

Fig. 2. Modeled swimming speed and forces over time. Instantaneous swimming speed, thrust, drag, and net thrust (combined thrust, drag, and buoyancy) for (*A*) Synchronous and (*B*) Asynchronous swimming.

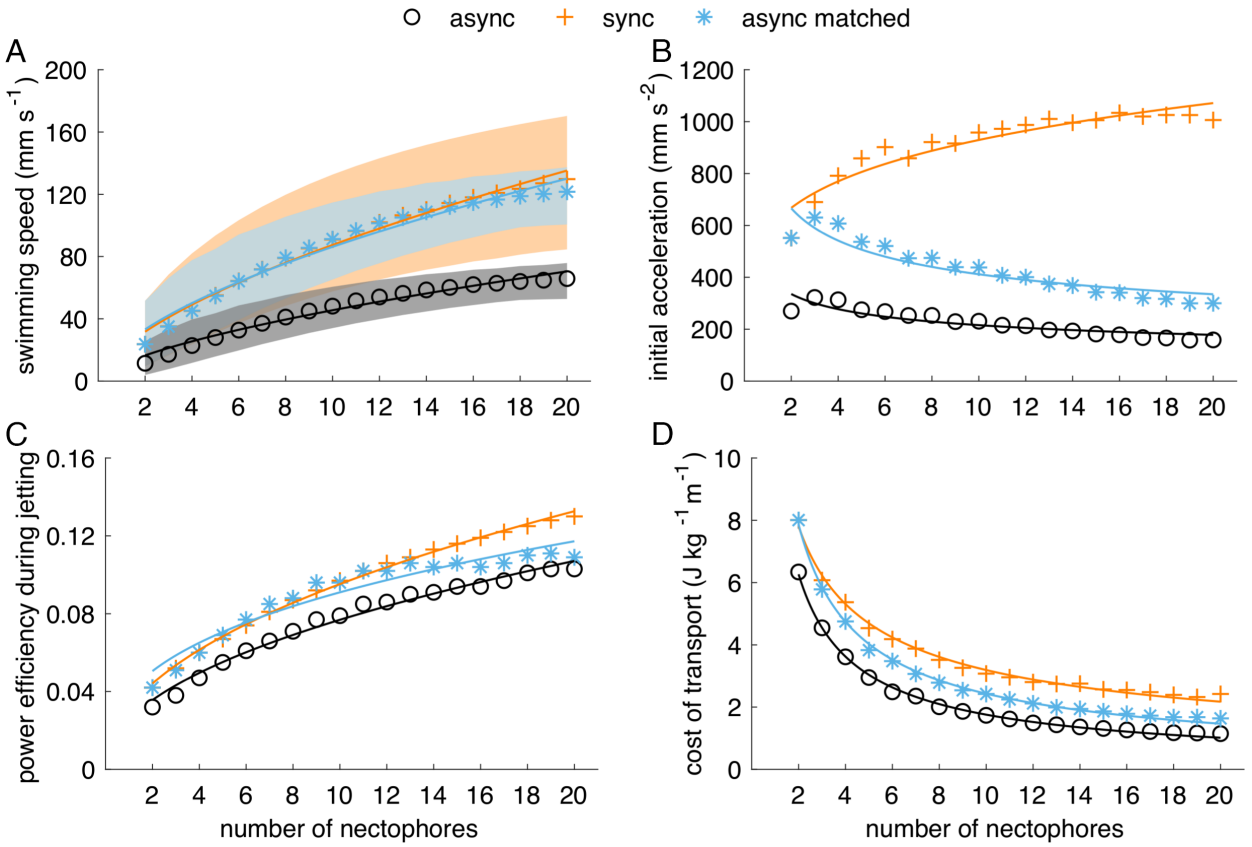

Fig. 3. Effects of colony length and swimming mode on swimming kinematics and cost of transport. (*A*) Swimming speed mean and range (envelope), (*B*) Initial acceleration, (*C*) Power efficiency during jetting, and (*D*) Cost of transport. For the "async matched" case, the model was run asynchronous but with thrust and drag parameters matched to the synchronous case. Compared to asynchronous swimming, synchronous swimming yielded higher mean and maximum swimming speeds and greater accelerations but also a higher cost of transport.

synchronous modes using data from videos and by comparing the thrust and drag parameters for each swimming mode in the model (*SI Appendix*, Table S1).

Using previously reported data (13, 16), we estimated maximum thrust per nectophore to be 60 μN, as described in supplemental materials (*SI Appendix*, Fig. S2). From videos, we measured contraction depths (expanded divided by contracted diameter) and durations and pulse frequencies for both swimming modes and found that only contraction depth differed significantly; contraction depth was approximately 1.4 times as high for synchronous as for asynchronous swimming (*t*-test $p = 0.01$; *SI Appendix*, Fig. S3). In the model, thrust for synchronous swimming was 0.9 times the expected value; thrust for asynchronous swimming was 0.5 times the expected value (*SI Appendix*, Table S1). Together, these results suggest that *N. bijuga* produces more thrust per nectophore during synchronous swimming.

Based on particle image velocimetry (PIV) analysis, we estimated the drag on the siphosome to be half that on the nectosome (*SI Appendix*, Fig. S4). From the model, the drag coefficient was higher than the initial estimate and 1.6 times higher for asynchronous than for synchronous swimming; the drag parameters in the model were 4.2 and 2.7 for asynchronous and synchronous swimming (Eq. **3**). The effect of a time-varying frontal area is not included in the model, but a synchronously pulsing nectosome has a smaller frontal area during contraction than an asynchronously pulsing one, which may help to explain the higher drag coefficient for asynchronous swimming. Although the drag coefficient was lower for synchronous swimming, absolute drag was often higher for synchronous swimming due to the higher swimming speeds (Fig. 2).

We performed a sensitivity analysis to compare the relative importance of frequency, thrust, drag, and mass in determining mean swimming speeds across a range of colony lengths in each swimming mode and the pairwise effects of thrust, drag, and mass on swimming speed for a colony with 12 nectophores (*SI Appendix*, Figs. S5 and S6). The mean swimming speed was most sensitive to thrust, followed by drag, frequency, and finally mass, based on the swimming speed ranges between the highest and lowest parameter values tested (*SI Appendix*, Table S3). Synchronous swimming speeds were more sensitive to changes in frequency, thrust, and drag than asynchronous swimming speeds but similarly sensitive to changes in mass. The greatest combined effect on swimming speed was found when varying thrust and drag together (*SI Appendix*, Fig. S6 *A* and *D*).

Together, these results suggest that the observed differences in swimming speed are primarily due to two factors: greater thrust production per nectophore and less drag in synchronous swimming. While both thrust and drag are likely important, the sensitivity analysis suggests that differences in thrust are more important than differences in drag in determining swimming speeds, particularly for longer colonies (*SI Appendix*, Fig. S5).

Swimming Performance. We used the model to calculate efficiency and hydrodynamic—as opposed metabolic—cost of transport (Fig. 3 *C* and *D* and *SI Appendix*, Fig. S7). Hydrodynamic efficiencies were higher for synchronous than asynchronous swimming for all colony lengths; alternate efficiency metrics

showed the same trend (*SI Appendix*, Fig. S7). The cost of transport, however, may be a better metric for swimming performance in this case because it is normalized by swimming speed, which is always higher for synchronous swimming; the cost of transport was consistently lower for asynchronous than for synchronous swimming.

The asynchronous-matched swimming case yielded similar mean swimming speeds to synchronous swimming but generally narrower swimming speed ranges and lower initial accelerations (Fig. 3*A*). The matched parameter case demonstrates that when swimming speeds are similar, synchronous swimming is more efficient for longer colonies (≥12 nectophores). The cost of transport was lower for asynchronous-matched than for synchronous swimming for all but the two nectophore colonies.

There are few published estimates of efficiency and cost of transport for siphonophores, but our modeled cost of transport for an *N. bijuga* colony with two nectophores swimming asynchronously, 6.3 J kg^{-1} m^{-1}, was similar to the 3 J kg^{-1} m^{-1} calculated by Bone and Trueman (21) for the calycophoran siphonophore *Abylopsis tetragona*, which has one full-sized and one reduced nectophore. *N. bijuga* colonies with five or more nectophores were found to have costs of transport less than 3 J kg^{-1} m^{-1} when swimming asynchronously, putting them toward the lower end of reported values for jet-propelled swimmers (2).

Effects of Colony Length. Increases in colony length provide swimming benefits for both asynchronous and synchronous swimming (Fig. 3). While mean swimming speeds increase for both swimming modes, it increases much more rapidly for synchronous swimming, more than threefold for an increase from 4 to 20 nectophores. Acceleration increases with colony length for synchronous swimming but decreases for asynchronous swimming. Efficiency increases, and the cost of transport decreases with colony length for both swimming modes.

Longer colonies benefit from lower costs of transport during asynchronous swimming and faster escapes during synchronous swimming. These relationships approach asymptotes as colony length increases, however, suggesting a limit to the hydrodynamic advantages of colony growth. In our videos of 36 *N. bijuga* colonies collected at Friday Harbor, only six colonies had more than 10 nectophores, and one colony had 20 nectophores. Mackie (22) reported that few *Nanomia* colonies from Friday Harbor had more than 15 nectophores.

Discussion

There is a common tradeoff in locomotion between proficiency (speed) and efficiency. This tradeoff can be seen when comparing taxa with different styles of locomotion. For example, hydromedusae taxa can be categorized based on their feeding strategies and corresponding swimming modes—slow-swimming "rowers" are cruising predators that swim continuously and efficiently, whereas fast-swimming "jetters" are ambush predators that swim intermittently and less efficiently (23, 24). A hydrodynamic analysis of the swimming of seven hydromedusae species showed that species could either swim proficiently (jetters) or efficiently (rowers), with morphological constraints likely preventing an individual hydromedusa from achieving both (24).

The appropriate balance of proficiency and efficiency for an individual organism can change, however, depending on context. For example, routine and long-distance locomotion favor efficiency, whereas prey capture and escape from predators favor proficiency. One way for an organism to match the balance of proficiency and efficiency to the context is to possess multiple gaits with varying balances of the two. Many fishes, for example, have routine and escape swimming gaits adapted to efficiency and speed, respectively (17, 18), whereas hydromedusae can change pulsation rates but have only a single gait.

By varying the timing of thrust propulsion by multiple propulsors, *N. bijuga* gains the ability to adapt its swimming to context analogously to the swimming gaits of fishes but without the associated high metabolic costs of a fish's neuromuscular system. While the existence of escape swimming modes with distinct neural pathways has long been documented for *N. bijuga* (e.g., ref. 22) and other cnidarians (reviewed in ref. 25), the performance of these swimming modes has received little attention. Here, we show that *N. bijuga* has context-specific swimming modes that mirror those seen in fishes. Furthermore, the exponents for swimming speed vs. colony length for both asynchronous and synchronous swimming in *N. bijuga* (0.78 and 0.79) are near the high end of the range for many fishes, for which swimming speed scales with length to the power of 0.50 for active swimming and 0.88 for burst swimming (26). *N. bijuga*'s ability to control the timing of propulsion by multiple propulsors gives it access to two swimming modes, synchronous swimming to maximize speed and asynchronous swimming to minimize energy consumption.

Distributed propulsion enables asynchronous and synchronous swimming modes with context-specific advantages, as demonstrated by the differences in swimming performance. For successful escape swimming, high accelerations and swimming speeds are crucial, and energy consumption is of secondary concern, particularly if swimming bouts are of short duration (*N. bijuga* often only swims synchronously for a few pulses). In addition to escaping capture, *N. bijuga* could use synchronous swimming to escape predation post capture, for example, from narcomedusae (20), as observed by Raskoff (27). Asynchronous swimming is used for routine swimming and vertical migration, activities in which energy consumption is important. When observed in large tanks for this study, *N. bijuga* used asynchronous swimming in two different ways. First, when *N. bijuga* was suspended nearly motionless, it periodically performed short asynchronous bouts, deploying its siphosome for fishing or adjusting its position in the water. Second, *N. bijuga* performed longer asynchronous bouts, moving up or down in the water column; this swimming behavior is likely also used in vertical migration (7, 19), but buoyancy regulation may play a role as well.

During a typical asynchronous swimming cycle, *N. bijuga* contracts its nectophores in opposite pairs, starting at the apex and progressing down the nectosome (Fig. 1*C*). This pattern of propulsion, in which multiple propulsors produce thrust in sequence in a wave that travels along an organism's body, is termed metachronal swimming (28). While research on metachronal swimming has typically focused on organisms that use paddles for propulsion, such as crustaceans, ctenophores, and polychaetes (29–31), many of the same principles apply to multijet swimming. An advantage of metachronal swimming, as compared to synchronous swimming, is that it distributes thrust production over the course of a swimming cycle, which dampens accelerations, leading to steadier swimming; we see this phenomenon in our measured and modeled instantaneous swimming speeds (Fig. 1 *C* and *D*) and in the swimming speed ranges produced by the model (Fig. 3*A*).

Salps—another group of multijet swimmers—provide a useful comparison to physonect siphonophores. Salps also swim in asynchronous and synchronous modes, but they swim asynchronously through uncoordinated pulsation by individual

zooids, each of which has an independent timing cycle (32) as opposed to the coordinated, metachronal asynchronous pulsation of physonect nectophores. For long salp colonies, coordinated and uncoordinated asynchronous swimming produce similar performance, but for shorter colonies, variations in propulsion timing can lead to constructive interference or "beating" that increases unsteadiness (32). Coordinated asynchronous swimming in physonect siphonophores, in contrast, distributes thrust more evenly over time.

Providing specific advice for vehicle design is beyond the scope of this study, but experimental pulsed single jet vehicles that operate within the Reynolds number range this study (*SI Appendix*, Fig. S1) have been tested (e.g., Re = 1,300–2,700 for 33), and there are general principles from this study that could be useful for vehicle research and design. Analogously to *N. bijuga*, a single underwater vehicle with multiple propulsors could use different modes to adapt to context. Our model test cases suggest strategies for tuning the behavior of a vehicle depending on the desired performance characteristics. A propulsion pattern mimicking the asynchronous case—in which thrust is low, and asynchronous—is best if power consumption is the primary concern because it minimizes the cost of transport. If speed is more important, the asynchronous-matched case—in which thrust is high and asynchronous—is likely the best because it decreases the cost of transport with only small losses in speed when compared to the synchronous case. Interestingly, the intuitive approach of producing high thrust synchronously (as represented by the synchronous case) may be the least useful, with its primary advantage being high initial acceleration.

Our results also suggest a general approach to selecting the number of propulsors an underwater vehicle should employ. Swimming speed, efficiency, cost of transport, and synchronous acceleration all improved with increasing colony lengths in our model, but these benefits approached asymptotes for the longest colonies (Fig. 3). For underwater vehicles with few propulsors, adding propulsors may provide large performance benefits, but when the number of propulsors is high, the increase in complexity from adding propulsors may outweigh the incremental performance gains.

The multijet strategy provides flexibility in the spatial and temporal distributions of propulsion. Multijet swimmers, such as *N. bijuga*, take advantage of this flexibility to increase their maneuverability, redundancy, and context-specific swimming performance.

Materials and Methods

Swimming Parameters from Videos. To compare asynchronous and synchronous swimming in *N. bijuga*, we measured or estimated relevant morphometric parameters and kinematic and hydrodynamic parameters for each swimming mode from video analyses and the literature. Laboratory videos of free-swimming *N. bijuga* were collected at Friday Harbor Laboratories between 2014 and 2021. Recording methods for videos taken before 2021, including camera specifications, fields of view, etc., were described previously (13, 16). Synchronous swimming was elicited by gently touching the siphosome with a stirring rod.

N. bijuga rarely swims asynchronously in the smaller filming vessels typically used for swimming studies, so, in order to capture additional asynchronous swimming events, several *N. bijuga* at a time were maintained in a large pseudo-kreisel tank (inner dimensions 71 cm height × 56 cm width × 34 cm depth) with natural flowing seawater (10–11°C, salinity 35–37) for one to several days, during which they often exhibited asynchronous swimming behavior, either spontaneously or after stimulation by cycling the room lights. Videos in the pseudo-kreisel were recorded at 60 frames per second using a Photron Nova R2 with a 60-mm macro lens and either back or oblique lighting.

Siphosome length (L) and maximum diameter (D) were measured from 133 brightfield videos of 36 colonies with between 4 and 20 nectophores (N). Siphosome length scaled approximately linearly with the nectophore count ($L = 1.64N + 0.68$ mm; $R^2 = 0.75$). There was no clear relationship between the siphosome maximum diameter and nectophore count ($R^2 < 0.001$; slope = 0.005 for a linear fit); the mean diameter was 5.5 mm (*SI Appendix*, Fig. S8).

Instantaneous swimming speeds (V) were measured from videos using the DLTdv 8 package (34) for MATLAB by tracking the pneumatophore (n = 13 asynchronous and 11 synchronous colonies). Swimming speeds were calculated from the vertical component of swimming velocity, and only videos in which the swimming direction was primarily upward were analyzed. For each sequence, we calculated the minimum, maximum, and mean swimming speed and categorized the sequence as asynchronous or synchronous. In videos in which swimming began from rest, the initial period of acceleration was excluded from mean and minimum swimming speed calculations.

We were unable to find published values for the weight or density of *N. bijuga* or a closely related species, so we estimated a density of ρ = 1,021 kg m^{-3}, slightly higher than the value we used for the seawater density (ρ_f = 1,020 kg m^{-3}), based on the observation that *N. bijuga* sinks slowly when not swimming. *N. bijuga* can alter its density by controlling the pressure in its gas-filled pneumatophore (14, 19) and possibly by altering the concentrations of heavy ions, such as sulfate, in bracts and other tissue (35), but because the focus of this study was short swimming bouts–during which changes in density should be minor–rather than vertical migration, we used a fixed value for density.

We calculated maximum thrust for nine nectophores using data from Costello et al. (13, their Figures 2 and 3). The most recently formed nectophores nearest to the pneumatophore produce less thrust than older nectophores farther from the pneumatophore (13), but we used the mean thrust per nectophore for simplicity.

To determine the timing of thrust production, we calculated time-varying thrust during the jetting period for a single nectophore using jet velocity and nectophore velum orifice kinematics data from Sutherland et al. (16, their Figure 4) using the formula:

$$F_t = \cos\theta \cdot v_{\text{jet}} \cdot \dot{m}_{\text{jet}} = \cos\theta \cdot v_{\text{jet}}^2 \pi \frac{d^2}{4} \rho_f, \quad [1]$$

where F_t is thrust, θ is the angle of the jet with respect to the nectosome major axis, v_{jet} is mean jet velocity, $\dot{m}_{\text{jet}}$ is the mass flow rate of the jet, d is the velum orifice diameter, and ρ_f is the density of seawater.

For a subset of asynchronous and synchronous videos (n = 9 asynchronous and 6 synchronous colonies), we recorded frame numbers and maximum diameters of nectophores at peak expansion and peak contraction to compare the depth and duration of contraction. We also calculated pulse frequencies for 19 asynchronously swimming and 10 synchronously swimming colonies.

Drag was calculated using the equation:

$$F_d = 0.5 \cdot \rho_f \cdot C_d \cdot A \cdot V \cdot |V|, \quad [2]$$

where is A is the frontal area of the nectosome, and C_d is a variable drag coefficient:

$$C_d = \frac{24}{Re} \cdot \left(1 + 0.15 \cdot Re^{0.687}\right) + \frac{0.42}{1 + 42500/Re^{1.16}}, \quad [3]$$

where $Re = VD/\nu$ is a Reynolds number based on the swimming speed, nectosome diameter (D), and the kinematic viscosity of the fluid (9.8×10^{-7} m^2 s^{-1}), an expression for drag on a sphere at $Re < 2 \times 10^5$ (36). Variable drag coefficient equations exist for other geometries, but their utility is limited by the need to estimate additional shape parameters (37). We also chose to use a fixed nectosome diameter in the model to limit the number of model parameters.

We treated the drag force (F_d) for the nectosome and siphosome separately. Drag on the siphosome was calculated using PIV analysis of a video sequence

of asynchronous swimming as described in the supplementary materials. Flow from the jets precluded a similar analysis for the nectosome. Instead, drag on the nectosome was calculated using Eq. **2** based on the frontal area–estimated as the area of a circle circumscribing the widest part of the nectosome. For comparison, we also ran the model using wetted nectosome surface area as the reference area in Eq. **2** but found that the results using the frontal area more closely matched experimental data (*SI Appendix*, Fig. S9).

Swimming Model. To further examine asynchronous and synchronous swimming across a range of swimming parameters, we developed a model relating drag, thrust, buoyancy, and mass to instantaneous swimming speeds (38). We calculated swimming speed by numerically solving the unsteady equation of motion (Newton's second law) in the swimming direction:

$$\frac{dV}{dt} = \frac{F_t - F_d + B}{m + \alpha\, m_f}, \qquad [4]$$

where V is swimming speed, t is time, F_t is the thrust force, F_d is the drag, $B = -(m - m_f) \cdot g$ is buoyancy, g is acceleration due to gravity, m is mass of the colony, and α is a constant which yields the added mass when multiplied by m_f, the mass of fluid displaced by the colony. We used a value of 0.1 for α, assuming an elongate spheroid (39, 40, p. 276). The value for the mass was based on the density (ρ) multiplied by the volume of the nectosome, which we estimated using the volume of a cylinder with the same length and diameter as the modeled colony. Because nectophores generate thrust in both jetting and refill phases, thrust for a single nectophore consisted of two components, one for each phase (16). Each component consisted of a Fourier series approximation of a square wave, which provided a differentiable function with a variable duty cycle. Total thrust for the colony was calculated by summing the functions for all nectophores; this approximation assumes that interactions between jets do not affect the total thrust generated. Quantifying the effects of these interactions is outside the scope of this study. Based on flow-field visualizations during synchronous swimming, the jets appear to be separated within a few jet diameters of the body (e.g., ref. 16, their Figure 1B), but jet interactions are likely to be more important for synchronous than for asynchronous swimming. For each model run, we solved Eq. **4** using MATLAB's ODE45 solver with variable step size. The model was run in two modes based on swimming modes observed in the videos. In the synchronous mode, all nectophores produce thrust simultaneously. In the asynchronous mode, pairs of nectophores produce thrust in sequence.

As a starting point, we parameterized the model based on values extracted from videos (Table 1). We then tuned the model to match measured swimming speeds by running the model in either asynchronous or synchronous swimming mode over a range of colony lengths from 2 to 20 nectophores and iteratively adjusting swimming parameters (thrust and drag) to minimize the summed root mean squared errors (RMSE) of mean, minimum, and maximum swimming speeds between the model and the videos. We also ran the model in asynchronous mode with synchronous parameters to directly compare the swimming modes without confounding effects; we refer to this mode as the asynchronous matched case.

Additionally, we tuned the model to match instantaneous speeds from particular asynchronous and synchronous video sequences. In this case, we adjusted the pulse frequency to match the measured pulse frequency for a particular video and tuned thrust, drag, and mass to minimize the RMSE between modeled and measured instantaneous swimming speeds.

Efficiency and Cost of Transport. We calculated a "power efficiency" during the jetting phase based on the ratio of power output P_o to power input P_i (41), where $P_i = F_t \cdot v_{\text{jet}}$, and P_o combines power losses due to drag and inertia:

$$P_o = F_d \cdot V + (m + \alpha m_f) V \frac{dV}{dt}. \qquad [5]$$

The hydrodynamic cost of transport was calculated as $\text{COT} = P_i / mV$, with units J kg^{-1} m^{-1} (41, 42); this metric for the cost of transport differs from the metabolic cost of transport in that it encompasses only energy consumption derived from fluid motion. Additional efficiency metrics are presented and described in the supplemental materials.

Data, Materials, and Software Availability. [Videos] data have been deposited in [Figshare] (10.6084/m9.figshare.19158326).

ACKNOWLEDGMENTS. Kayla Nease assisted with video analyses. Matt K. Fu and Alejandro Damian-Serrano provided useful comments on the manuscript. Caitlyn Webster provided the illustration for Fig. 1*A*. Funding was provided by the Gordon and Betty Moore Foundation (8835) and the National Science Foundation awarded to SPC (2100156 and 2114169) and JHC (2100705 and 2114170) and BJG (2100703).

Author affiliations: [a]Oregon Institute of Marine Biology, University of Oregon, Eugene, OR 97403; [b]Department of Integrative Biology, University of South Florida, Tampa, FL 33620; [c]Marine Biology and Environmental Science, Roger Williams University, Bristol, RI 02809; [d]Biology Department, Providence College, Providence, RI 02918; and [e]Graduate Aerospace Laboratories and Mechanical Engineering, California Institute of Technology, Pasadena, CA 91125

1. L. A. Ruiz, R. W. Whittlesey, J. O. Dabiri, Vortex-enhanced propulsion. *J. Fluid Mech.* **668**, 5–32 (2011).
2. B. J. Gemmell *et al.*, Cool your jets: Biological jet propulsion in marine invertebrates. *J. Exp. Biol.* **224**, jeb222083 (2021).
3. K. R. Sutherland, L. P. Madin, Comparative jet wake structure and swimming performance of salps. *J. Exp. Biol.* **213**, 2967–2975 (2010).
4. K. R. Sutherland, B. J. Gemmell, S. P. Colin, J. H. Costello, Maneuvering performance in the colonial siphonophore. *Nanomia bijuga. Biomimetics* **4**, 62 (2019).
5. H. Jiang, J. H. Costello, S. P. Colin, Fluid dynamics and efficiency of colonial swimming via multijet propulsion at intermediate reynolds numbers. *Phys. Rev. Fluids* **6**, 013103 (2021).
6. G. M. Mapstone, Global diversity and review of siphonophorae (cnidaria: Hydrozoa). *PLoS One* **9**, e87737 (2014).
7. E. G. Barham, Deep scattering layer migration and composition: Observations from a diving saucer. *Science* **151**, 1399–1403 (1966).
8. A. Damian-Serrano *et al.*, Characterizing the secret diets of siphonophores (cnidaria: Hydrozoa) using DNA metabarcoding. *PloS One* **17**, e0267761 (2022).
9. J. Purcell, Dietary composition and diel feeding patterns of epipelagic siphonophores. *Marine Biol.* **65**, 83–90 (1981).
10. Topical Stud, B. H. Robison, K. R. Reisenbichler, R. E. Sherlock, J. M. Silguero, F. P. Chavez, Seasonal abundance of the siphonophore, Nanomia bijuga, in Monterey Bay. *Deep Sea Res. Part II. Oceanogr.* **45**, 1741–1751 (1998).
11. G. Mackie, P. Pugh, J. Purcell, "Siphonophore biology" in *Advances in Marine Biology* (Elsevier, 1988), vol. 24, pp. 97–262.
12. C. Dunn, Siphonophores. *Curr. Biol.* **19**, R233–R234 (2009).
13. J. H. Costello, S. P. Colin, B. J. Gemmell, J. O. Dabiri, K. R. Sutherland, Multi-jet propulsion organized by clonal development in a colonial siphonophore. *Nat. Commun.* **6**, 1–6 (2015).
14. W. Jacobs, Beobachtungen über das schweben der siphonophoren. *Zeitschrift für vergleichende Physiologie* **24**, 583–601 (1937).
15. G. V. Pickwell, E. G. Barham, J. W. Wilton, Carbon monoxide production by a bathypelagic siphonophore. *Science* **144**, 860–862 (1964).
16. K. R. Sutherland, B. J. Gemmell, S. P. Colin, J. H. Costello, Propulsive design principles in a multi-jet siphonophore. *J. Exp. Biol.* **222**, jeb198242 (2019).
17. P. Domenici, M. E. Hale, Escape responses of fish: A review of the diversity in motor control, kinematics and behaviour. *J. Exp. Biol.* **222**, jeb166009 (2019).
18. K. T. Du Clos *et al.*, Thrust generation during steady swimming and acceleration from rest in anguilliform swimmers. *J. Exp. Biol.* **222** (2019).
19. E. G. Barham, Siphonophores and the deep scattering layer. *Science* **140**, 826–828 (1963).
20. C. A. Choy, S. H. Haddock, B. H. Robison, Deep pelagic food web structure as revealed by in situ feeding observations. *Proc. Roy. Soc. B: Biol. Sci.* **284**, 20172116 (2017).
21. Q. Bone, E. Trueman, Jet propulsion of the calycophoran siphonophores chelophyes and abylopsis. *J. Marine Biol. Assoc. U. K.* **62**, 263–276 (1982).
22. G. O. Mackie, Analysis of locomotion in a siphonophore colony. *Proc. Roy. Soc. Lond. Ser. B Biol. Sci.* **159**, 366–391 (1964).
23. S. P. Colin, J. H. Costello, Morphology, swimming performance and propulsive mode of six co-occurring hydromedusae. *J. Exp. Biol.* **205**, 427–437 (2002).
24. J. O. Dabiri, S. Colin, K. Katija, J. H. Costello, A wake-based correlate of swimming performance and foraging behavior in seven co-occurring jellyfish species. *J. Exp. Biol.* **213**, 1217–1225 (2010).
25. GO Mackie, "Fast pathways and escape behavior in cnidaria" in *Neural Mechanisms of Startle Behavior* (Springer, 1984), pp. 15–42.
26. J. T. Bonner, T. A. McMahon, *On Size and Life* (Scientific American Library, 1983).
27. K. Raskoff, Foraging, prey capture, and gut contents of the mesopelagic narcomedusa solmissus spp. (cnidaria: Hydrozoa). *Marine Biol.* **141**, 1099–1107 (2002).
28. E. Knight-Jones, A. Macfadyen, "The metachronism of limb and body movements in annelids and arthropods" in *Proceedings of XVth International Congress of Zoology* (1959), pp. 969–971 .
29. S. P. Colin *et al.*, The role of suction thrust in the metachronal paddles of swimming invertebrates. *Sci. Rep.* **10**, 17790 (2020).

30. D. Murphy, D. Webster, S. Kawaguchi, R. King, J. Yen, Metachronal swimming in antarctic krill: Gait kinematics and system design. *Marine Biol.* **158**, 2541–2554 (2011).
31. M. L. Byron *et al*., Metachronal motion across scales: Current challenges and future directions. *Integr. Comp. Biol.* (2021).
32. K. R. Sutherland, D. Weihs, Hydrodynamic advantages of swimming by salp chains. *J. Roy. Soc. Interface* **14**, 20170298 (2017).
33. A. A. Moslemi, P. S. Krueger, Propulsive efficiency of a biomorphic pulsed-jet underwater vehicle. *Bioinspir. Biomim.* **5**, 036003 (2010).
34. T. L. Hedrick, Software techniques for two-and three-dimensional kinematic measurements of biological and biomimetic systems. *Bioinspir. Biomim.* **3**, 034001 (2008).
35. R. R. Bidigare, D. C. Biggs, The role of sulfate exclusion in buoyancy maintenance by siphonophores and other oceanic gelatinous zooplankton. *Comp. Biochem. Physiol. Part A: Physiol.* **66**, 467–471 (1980).
36. R. Clift, W. H. Gauvin, *Proceedings of CHEMECA 1970* (1970), vol. 1, pp. 14–28.
37. E. Loth, Drag of non-spherical solid particles of regular and irregular shape. *Powder Technol.* **182**, 342–353 (2008).
38. S. Biringen, C. Y. Chow, *An Introduction to Computational Fluid Mechanics by Example*. (John Wiley spsampsps Sons, 2011).
39. H. Lamb, *Hydrodynamics* (Dover, New York, 1945), pp. 134–139.
40. S. Vogel, *Life in Moving Fluids* (Willard Grant Press, Boston, 1981).
41. T. L. Daniel, Mechanics and energetics of medusan jet propulsion. *Can. J. Zool.* **61**, 1406–1420 (1983).
42. V. A. Tucker, The energetic cost of moving about: Walking and running are extremely inefficient forms of locomotion. Much greater efficiency is achieved by birds, fish–and bicyclists. *Am. Sci.* **63**, 413–419 (1975).